JVI
Journals.ASM.org

An Overview of the Vaccinia Virus Infectome: a Survey of the Proteins of the Poxvirus-Infected Cell

Wayne Chou, Tuan Ngo, and Paul D. Gershon

Department of Molecular Biology and Biochemistry, University of California—Irvine, Irvine, California, USA

We have quantitatively profiled the proteins of vaccinia virus-infected HEK293T cells early and late during vaccinia virus infection. Proteins corresponding to 4,326 accessions were identified, the products of 3,798 genes. One hundred thirty-six of the proteins were vaccinia virus-encoded (~64% of the known vaccinia virus proteome). The remaining accessions were from the host cell. A total of 3,403 of the 4,326 accessions could be confidently quantitated at the precursor peptide level. Although vaccinia virus gene products spanned the entire abundance dynamic range of the cellular proteome, nearly all of the proteome dynamics observed as a result of infection were manifest in the virus gene products with very little plasticity in the host cell proteome. The vaccinia virus gene products could be grouped into four kinetic classes (i.e., four combinations of pre- and postreplicative expression). These protein kinetic classes reflected, almost entirely, the corresponding gene classes within the recently characterized vaccinia virus transcriptome map. The few cellular gene products that showed notable changes in abundance upon vaccinia virus infection were concentrated largely in just a few functional groups. After all of the quantitated cellular gene products were assigned to Gene Ontology (GO)-specific groups, quantitation values for a number of these GO-specific groups were significantly skewed toward over- or underabundance with respect to the global distribution of quantitation values. Quantitative analysis of host cell functions reflected several known facets of virus infection, along with some novel observations.

Poxviruses are among the largest and most complex of animal viruses, have double-stranded linear DNA genomes, and replicate within the cytoplasm of the infected cell. Vaccinia virus is the prototypical member of the orthopoxvirus genus and of the *Poxviridae* as a whole. Vaccinia virus is notable in being not only the smallpox vaccine but also a very close evolutionary relative of the smallpox virus. Of the 200 or so genes carried by the vaccinia virus, the early class is expressed immediately after entering the host cell, from the still encapsidated genome. The early phase is followed by genome replication, synthesis of intermediate- and late-class mRNAs, the complex processes of new virion assembly, and then cell exit.

Multiple studies have characterized the global kinetics of mRNA synthesis and homeostasis during orthopoxvirus infection. Hybridization studies showed that, by 2 h and 7 h following high-multiplicity infection of HeLa cells with vaccinia virus, 50 to 60% and 80 to 90%, respectively, of the total poly(A)$^+$ RNA was virus specific (5). More recently, deep sequencing of vaccinia virus and host cell transcriptomes showed that, at 4 h postinfection of HeLa cells, 25 to 55% of poly(A)$^+$ RNA sequences were viral (61, 62, 63). Although overall amounts of mRNA were comparable in infected and uninfected cells, the proportion attributable to the virus was shown to change (62). In A594 cells infected with a virus very similar to vaccinia virus, namely, rabbitpox virus, a decline in overall cellular mRNA levels was reported beginning at 2.5 hpi, and, by 5 hpi, mRNA levels were drastically lower for the majority of cellular genes (8). In the above literature, host cell mRNA degradation has been interpreted as a driving force for these observations, and infection is therefore clearly accompanied by a progressive cessation of host mRNA synthesis and the degradation of host cell mRNA (5, 11, 62).

With regard to individual viral and cellular transcripts, steady-state levels have been investigated by microarray and deep-sequencing studies. Despite the overall drop in steady-state levels of host mRNAs after the infection of A549 cells with rabbitpox virus (8), mRNA levels were shown to be elevated between 1 and 2.5 h postinfection for some transcripts, namely, core histones, CYR61 (cysteine-rich, angiogenic inducer, 61), and EEF1A1 (eukaryotic translation elongation factor 1 alpha subunit isoform 1). At 5 h postinfection, levels of mRNAs were shown to increase for heat shock proteins, the transcription factor c-*fos*, and a proline/glutamine-rich splicing factor. Additional genes were differentially abundant between wild-type and serpin-deleted rabbitpox strains. In a microarray study of HeLa cellular mRNAs after infection with vaccinia virus for 2, 6, and 16 h, Guerra (21) found seven apparent kinetic patterns among 15,000 human genes in which most cellular transcripts showed a pattern of decreasing abundance during infection. Nonetheless, some host cell transcripts appeared more abundant at 2 h, and a subset of these (~4.6%) remained high (or increased further) at 6 h. A subset of the latter (37 transcripts or 2.8%) remained high even at 16 h. The latter group included genes for Wiskott-Aldrich syndrome protein (WASP) family member WASF1, thymosine, adenosine A2a receptor, glutamate decarboxylase 2, CD-80 antigen, KIAA0888 protein, selenophosphate synthetase, pericentrin, and attractin. A microarray study by Ludwig et al. (34) examined the role of viral factor E3L in the infection of human HeLa cells with vaccinia virus (MVA strain) and identified differentially expressed host genes. These authors identified a cluster of cellular genes with significantly increased intensities exclusively in cells infected with an E3L-deficient (MVA-E3L$^-$) strain of vaccinia virus, including

Received 23 August 2011 **Accepted** 8 November 2011
Published ahead of print 16 November 2011
Address correspondence to Paul D. Gershon, pgershon@uci.edu.
Supplemental material for this article may be found at http://jvi.asm.org/.

doi:10.1128/JVI.06084-11

transcripts for interleukin-6, growth arrest and DNA damage-inducible protein b (Gadd45b), activating transcription factor 3 (ATF3), basic-leucine zipper (bZIP) transcription factor AP-1 (JUN), dual-specificity protein phosphatases, and the zinc finger protein SNAIL2.

More recently, a deep-sequencing study of the vaccinia virus-infected HeLa cell poly(A)$^+$ transcriptome, which included more than 14,000 host cell mRNAs (62), showed that 50 to 75% of individual cellular transcripts had decreased in abundance by 4 h postinfection. An increase in abundance, however, by 2-fold or more was demonstrated for 119 cellular mRNAs whose functions fell into various groups including the NF-κB cascade, apoptosis, inhibition of apoptosis, signal transduction, and ligand-mediated signaling. At 4 h, the only statistically significant overrepresented category was chromatin packaging and remodeling. Among the vaccinia virus transcripts that were characterized, host interactors were shown to be expressed mostly early (62).

With regard to host cell gene expression at the protein level, pulse-labeling/SDS-PAGE studies have shown that, within 20 min of vaccinia virus infection, the major new proteins were viral in origin against a background of host cell protein synthesis that appeared to tail away (19, 39). Despite the above studies, host cell protein homeostasis at the level of individual host cell proteins has not been addressed. Here, using a quantitative protein mass spectrometry approach, we have compared the steady-state levels of individual proteins in uninfected HEK293T cells and vaccinia virus infection in the presence and absence of AraC, providing a vaccinia virus infectome.

MATERIALS AND METHODS

Cell culture and infection. HEK293T cells were grown to confluence in Dulbecco's modified Eagle's medium (DMEM) supplemented with 5% fetal bovine serum (FBS). Three T150 flasks were employed for each of the three conditions examined, namely, mock infection, infection, and infection in the presence of AraC (40 μg/ml). Cells were infected with purified vaccinia virus at a multiplicity of 20 PFU per cell following standard protocols (18). After incubation of all flasks in parallel for 20 h at 37°C, cell sheets were examined by light microscopy, then very gently washed with 25 ml of phosphate-buffered saline (PBS) twice, then examined again by microscope for integrity, and then scraped in 25 ml of PBS, followed by low-speed centrifugation, removal of supernatant, and snap-freezing.

Protein extraction and concentration determination. Cell pellets were dissolved in TRIzol (Invitrogen, Inc.), and protein was precipitated following the manufacturer's protocol. Protein pellets were redissolved in 4% SDS followed by three rounds of heating at 95°C (5 min) and sonication (5 min). Protein concentration was then determined by bicinchoninic acid (BCA) (Thermo Pierce, Rockford, IL) as described by the manufacturer.

Protein digestion. The procedure of Wisniewski et al. (59) was followed, with minor modifications. Briefly, 25 μg of each protein solution (mock infected, early [AraC] infected, and late infected) was supplemented with 200 μl of 8 M urea in 0.1 M triethylammonium bicarbonate (TEAB; Sigma-Aldrich, St. Louis, MO), pH 8.5, and each mixture was added to a YM-30 filter (Millipore, Inc.), followed by centrifugation at 14,000 × *g* at room temperature for 15 min. Then, 50 μl of thiol capping solution (5 mM Tris 2-carboxyethyl phosphine [TCEP; ThermoFisher-Pierce, Rockford, IL], 50 mM iodoacetamide [Sigma-Aldrich], 8 M urea) was added to the filter, followed by vortexing at low speed for 1 min; the sample was then incubated in the dark at room temperature for 20 min. Filters were then washed twice with 0.1 ml of 8 M urea in 100 mM TEAB (pH 8.5), followed by two washes with 0.1 ml of 0.1 M TEAB (pH 8.5). Trypsin (Sigma) was then added to each filter in 120 μl of 0.1 M TEAB (pH 8.5) at an approximate enzyme-to-substrate ratio of 1:100 (wt/wt). Samples were then incubated at 37°C for 4 h, followed by the addition of a second, equivalent aliquot of trypsin and overnight incubation at 37°C. The resulting peptide solution was spun from the filter and chased out with 50 μl of 0.5 M NaCl in water.

Dimethyl labeling and peptide fractionation. A total of 170 μl of trypsin digest was subjected to evaporation under vacuum before it was redissolved in 0.1 ml of 0.1 M TEAB (pH 8.5). Samples were then labeled with light-, intermediate-, and heavy-isotope-enriched dimethyl groups (4). Ten micrograms (equivalents) of peptides from each of the three labeled samples were combined, and the resulting peptide mixture was fractionated as described previously (27), eluting strong cation exchange material with 14 cuts of ammonium acetate, pH 2.7 (17.5, 20, 27.5, 35, 42.5, 50, 60, 70, 80, 90, 100, 230, 360, and 500 mM with respect to $NH4^+$; each step containing 30% CH_3CN). Each salt cut (with the exception of 500 mM) was subject to volume reduction to approximately 2 μl, followed by the addition of 25 μl of 0.1% ammonium hydroxide. The resulting peptide solutions were applied to a filter comprising styrene divinylbenzene (SDB) copolymer modified with sulfonic acid (3M, Inc.) that had been conditioned with 0.1% NH_4OH. After the filter was washed with 0.1% NH_4OH, peptides were eluted from SDB in three fractions (10, 20, and 80% CH_3CN in 0.1% NH_4OH) as described previously (27). The 500 mM salt cut was desalted using SDB and then eluted with 80% CH_3CN only. Each fraction was subjected to volume reduction under vacuum to <1 μl before volume adjustment to 10 μl with 0.1% formic acid (FA) for nano-liquid chromatography-tandem mass spectrometry (nanoLC-MS/MS) analysis.

NanoLC-MS/MS. The above fractions were analyzed via nanoLC-MS/MS using a linear trap quadrupole (LTQ) mass analyzer (Thermo Fisher Scientific, Rockford, IL) coupled to a Waters 600 high-performance liquid chromatography (HPLC) pump (Waters, Milford, MA) and Famos autosampler (Dionex, Sunnyvale, CA). C_{18} materials (MAC-MOD, Chadds Ford, PA) were pressure packed into a laser-pulled nanospray tip (15 cm by 75-μm internal diameter). Mobile phases were 0.1% FA in water (solvent A) and 0.1% FA in CH_3CN (solvent B). Gradients were run at a split flow rate of ~50 nl/min, with the active portion of the gradient running from 2% to 35% solvent B in solvent A, over 220 min. MS data were acquired in profile mode, with enhanced scan resolution, with the three most abundant precursor ions selected for MS/MS, and with dynamic exclusion.

Protein identification and quantitation. Spectral peak processing employed Mascot Distiller (version 2.3.2.0; Matrix Science, London, United Kingdom) with LCQ_plus_zoom.opt parameters and a precursor mass tolerance of 1.2 Da. Searches were against a custom library comprising all Internation Protein Index (IPI)-human isoform accessions combined with vaccinia virus accessions (fasta file for the latter downloaded from http://www.poxvirus.org). Additional searches were made against Swiss-Prot (release 57.1; selecting human and vaccinia virus taxonomy). The searches employed the following criteria: as fixed modification, cysteine carbamidomethylation; as variable modifications, methionine oxidation; and as exclusive modifications, heavy, intermediate, and light dimethyl labels selected for both N terminus and lysine side chain (4). A Mascot significance threshold (expectation score) of 0.05 was applied to all identified peptides, and, prior to quantitation, peptide lists were also filtered according to the Mascot identity threshold (so that only the most confidently identified peptides were quantitated). Spectral quantitation employed Mascot Distiller, which detected correlating dimethylated peptide peaks within a 15-s maximum-allowable deuteric shift in elution time. For each mass spectral peak, theoretical isotopic distribution models were fit to experimental isotopologues, followed by integration of peak areas under the model, followed by calculation of area ratios for correlating dimethylated peptide peaks (simple ratio method). Quantitation ratios for an extracted ion chromatogram (XIC) peak were the means of the individual values calculated for each scan across the peak. The statistical parameters for the fit between model and spectrum were calculated for individual spectra (standard error) and for the summed XIC as a whole

(correlation and fractional tolerance). Quantitation data for all confidently identified peptides were exported from Distiller for each nanoLC-MS/MS run independently and then merged using in-house software (PDMQ, P. D. Gershon, unpublished). Using PDMQ, merged data were subjected to an initial (automated) round of quality filtering on the basis of Mascot Distiller's statistical parameters (standard error of <999, fractional tolerance of >0.5, and correlation of >0.9). For each pairwise combination of samples within the three-sample set, a relative quantitation ratio was then derived for each peptide species as a geometric mean of Distiller's ratio values for individual data acquisitions, within the experiment, of the same peptide. For protein accessions that were quantitated on the basis of a single peptide species only (monopeptide quants), the resulting values were used directly as the quant ratio values for the protein accession. For protein accessions quantitated on the basis of multiple peptide species (multipeptide quants), the quant ratio for the protein was a weighted geometric mean of the peptide species' geometric means. Six continuous distributions (three sample pairs, each as a monopeptide and multipeptide distribution) of protein quant ratio values, from lowest to highest ratio value in the data set, were charted (y) against the corresponding protein accession (x). In the case of multipeptide protein quants, these charts included all individual peptide species means, which could be broken out, in turn, to show values for individual mass spectral acquisitions. As a second level of quality filtering, outlying quant values for individual acquisitions were picked from the above charts for verification or elimination via visual inspection of the raw MS spectral segments that had been used in the original quantitation (above), according to systematic rules given below, followed by a recalculation of the distributions. This process was iterated until all apparent outlying acquisitions from within the lower and upper 10th percentiles of each multipeptide distribution, along with the lower and upper 100 values in each monopeptide distribution, had been either verified or culled. All other annotation and analysis functions described here used PDMQ. For the analyses shown in Fig. 5 and Fig. S3 in the supplemental material, protein functions were assigned manually, mostly from UniProtKB's general annotation/function field.

Objective criteria for the visual verification or exclusion of spectral quant data. The identification scan should be within 10 MS scans or 30 s (whichever is smallest) of the integration region of the XIC. In addition, a simple majority (50% + 1) of scans within the integration region of the XIC should obey the following rules: (i) apparent charge must be 2+ or 3+;(ii) highest quantitated signal-to-noise ratio should be at least 3:1; (iii) no interfering peaks overlap the dimethyl isotopic triplet; (iv) experimental spectral profile visually correlates with Mascot Distiller's integration model.

RESULTS

Data acquisition and quantitation—methodology. In this study, the relative abundances of individual proteins between pairs of cell extracts was deduced by quantitative mass spectrometry. Relative quantitation by mass spectrometry is facilitated by differential isotope tagging since the resulting mass offsets, resident in the atomic nucleus, are clearly detectable in mass spectra yet have no secondary effects with regard to compound chemistry or ionizability. Here, differential isotopic labels were introduced by dimethyl labeling of peptides' N termini and lysine side chains (4). HEK293T cells were cultured under three sets of conditions, namely, uninfected, infected with vaccinia virus (WR) at high multiplicity for 20 h in the presence of cytosine arabinoside (AraC), and infected with vaccinia virus (WR) at high multiplicity for 20 h in the absence of inhibitors. After cells were harvested and washed, three protein extracts were generated, and 10 μg of protein from each extract, representing equivalent, cellular wet weight, was digested to peptides. After differential isotope labeling, the three labeled samples were combined, and the desalted mixture was subjected to two sequential stages of peptide fractionation (42 fractions total). The third and final stage of peptide fractionation comprised nanoLC-MS and nanoLC-MS/MS of each of the 42 peptide fractions in turn.

TABLE 1 Summary of data acquisition and quantitation[a]

Parameter	Value for the parameter
Acquisition	
Data acquisition time (days)	~11
No. of mass spectra acquired	~565,000
No. of successful MS/MS acquisitions in the Mascot data set	31,431
No. of unique peptide sequences in the Mascot data set	7,363
No. of unique accessions in the Mascot data set	4,326
FDR (%)[b]	3.84/1.54
Quantitation	
No. of unique precursor triplets quantitated in the data set	19,108
No. of assigned peptide sequence/fraction combinations in initial Mascot Distiller output	18,261
Total no. of frac/seq assignments after matrix fill	38,669
No. of assignments that were keratin	346
No. of assignments that passed keratin, machine filtering, visual inspection	30,149
Total no. of accessions that passed all filters	3,403
No. of multipeptide accessions	1,644
No. of monopeptide accessions	1,759

[a] Confident peptide identification (Mascot expectation score of <0.05) was furnished by a total of 31,431 MS/MS spectra. From these, 19,108 precursor-level isotopic triplets were subjected to modeling/quantitation (representing an average of ~1.64-fold redundancy in dimethyl isotopologues sent for MS/MS fragmentation). These represented 18,261 unique peptide sequence/chromatographic fraction combinations (representing ~4.6% average redundancy with regard to peptide sequence reacquisition per fraction, typically due to methionine oxidation). A total of 7,363 unique peptide sequences were represented within the quantitation data set representing, on average, a 2.48-fold redundancy in successful peptide reacquisition between chromatographic fractions. The complete data set covered 4,326 unique acquisitions within the vaccinia virus/IPI-human combined database, with 120 of these being vaccinia virus and the remainder human. These represented the products of 3,798 genes within 3,210 gene families. Peptide quantitation values corresponding to peptide sequences that had been applied to different (albeit related) accessions in searches of different chromatographic fractions were subsequently cross-applied to all relevant accessions over the data set as a whole. In this manner, the number of sequence/fraction combinations assigned in the initial data set (18,261) expanded to 38,669. The number of these that passed filtering on the basis of quantitation parameters (keratin peptides; machine filtering; visual inspection of quantitation outliers from which 1,287 spectral segments were visually inspected, with 353 accepted and 934 rejected) totaled 30,149 sequence/fraction combinations representing 3,403 unique accessions. Of these, 1,644 were represented by multiple peptide species per accession; the remaining 1,759 were represented by one peptide species only (albeit often more than one acquisition of the peptide species). Of the 3,404 confidently quantitated proteins, 1,292 could be assigned to the GO node cellular component\cell part\membrane, indicating that 38% of our confidently quantitated data set comprised membrane proteins, not inconsistent with the 30% or so of proteomes generally that may be regarded as membrane proteins (1).

[b] The first value is for accessions greater than homology plus identity thresholds; the second value is for identity alone.

Table 1 summarizes acquisition and quantitation results. The 31,431 MS/MS acquisitions scoring better than the Mascot expectation score threshold of 0.05 represented 7,363 unique peptide sequences among 4,326 unique accessions. The latter were from a combined database comprising IPI-human entries appended with accessions from vaccinia virus strain WR. A total of 120 of the 4,326 were vaccinia virus entries (see Table S1 in the supplemental material), representing approximately ~57% of the 212 gene

products encoded by vaccinia virus strain WR (counting duplicated genes once only). The false discovery rate (FDR) for the search was 4.91% (for accessions scoring above identity and homology thresholds) and ~1 to 2% (for accessions scoring above the identity threshold alone). IPI-human is an isoform database. When the search was repeated against Swiss-Prot (human plus vaccinia virus taxonomy selected), search results represented the products of 3,798 genes in 3,210 gene families (identity plus homology FDR, 3.84%; identity FDR, 1.54%), including 133 genes of vaccinia virus. This proteome contained single-peptide hits to the apparent products of two small, uncharacterized open reading frames (ORFs), YVDF_VACCW (41) and YH07_VACCW (32), which do not have corresponding VACWR designations and whose expression, as far as we are aware, has not previously been reported. However, since the respective peptides could have originated from human AKAP9 [(I/L)SLIEK] and VACWR013 (FTCVLTTIDGVSK), of which YVDF_VACCW is a truncated version, they are discounted. The Swiss search and the combined IPI and Swiss searches (136 hits), therefore, covered ~63% and ~64%, respectively, of vaccinia virus strain WR's 212-member proteome.

The 3,383 human genes represent ~15% of the human genome where, arguably, 50% (10,900 genes [35, 59]) might be expected to be expressed in a specific cell type. Insofar as this was a data-dependent experiment selecting peptides for MS/MS from high to low abundance, our host cell proteome may therefore represent approximately the top one-third of the total number of expressed proteins.

The 19,108 isotopic triplets in precursor spectra (Table 1) were subjected to quantitation by area integration. Since each of the 42 LC fractions was subjected to database searching independently, quantitation triplets corresponding to peptide sequences that had been applied to different (albeit related) accessions in different fractions were subsequently cross-applied to all relevant accessions over the data set as a whole. The resulting peptide quantitation data set was then machine filtered according to parameters relating to spectral quality and goodness of fit between data and isotopologue models (see Materials and Methods). From the filtered data, six distributions of relative quantitation ratios were drafted, corresponding to the three pairs of samples (early/mock, late/mock, and late/early, representing relative abundance ratios of each protein in the original samples), and for each accession relative quantitation ratios were assigned to one of two distributions on the basis of whether the accession was quantitated on the basis of multiple peptide species (multipeptide distributions) or just one peptide species (monopeptide distributions). Multiple rounds of visual inspection focused on the 10% of accessions present at either tail of each multipeptide distribution, along with the terminal 100 accessions from each monopeptide distribution. For these accessions, raw mass spectral segments (see, e.g., Fig. S1 in the supplemental material) were inspected for all individual peptide acquisitions whose quant ratios were outliers, followed by acceptance or rejection of their data points based upon objective criteria (see Materials and Methods). Acceptance/rejection of batches of data points was followed by the recalculation of distributions. This process was repeated iteratively until all outlying values had been either confirmed or eliminated from the data set. In addition, within protein families, raw spectra corresponding to peptide species shared between family members that led to significant variation between family members were also visually inspected followed by acceptance/rejection. In this manner, ~1,300 triplets in all (~6.5% of the total data set) were reviewed visually. The data set remaining after all of the processes described above was considered to be our confident quantitation data set and is analyzed below.

Quantitation data set: overview. Figure 1 shows the final multipeptide distributions. In the following analysis, conclusions were drawn solely on the basis of the multipeptide quant ratio distributions (Fig. 1), with the monopeptide distributions (data not shown) serving merely as confirmation where relevant. It can be seen that infection is associated with much more dramatic levels of protein overabundance with respect to the median of each distribution than underabundance. The overabundant proteins were, overwhelmingly, the vaccinia virus ones, while those whose steady-state levels remained between the 10th and 90th percentiles during infection were, by and large, the cellular ones.

Vaccinia virus gene products. A total of 104 of the 136 confidently identified vaccinia virus gene products remained in the final (filtered) quantitation data set: 70 in the multipeptide distributions and the remaining 34 in the monopeptide distributions. Figure 2 (upper panels) was derived from Fig. 1 by stripping away host cell accessions, showing quant ratio distributions for vaccinia virus accessions only, against the median and 10th and 90th percentile lines for all accessions. Lower panels show the equivalent for the monopeptide distributions. Vaccinia virus accessions were dramatically skewed to the top ends of all distributions, particularly during the late phase of infection. In terms of proteome dynamics therefore, vaccinia virus proteins underwent the most striking abundance changes during infection: 45 of the 46 most abundant proteins late, with respect to early, were vaccinia virus proteins. Similarly, only a single cellular protein was present within the 69 proteins present at the upper end of the late/mock distribution, with the remainder being from vaccinia virus. Therefore, the virus proteome represented almost the entirety of proteome dynamics during infection (at least within the most abundant ~56% and 33% of the vaccinia virus and host cell proteomes, respectively, as discussed above). These data provided a key conclusion of this study, namely, that vaccinia virus infection is accompanied by the appearance of vaccinia virus proteins against a relatively stable host cell proteomic background. This would be consistent with the expected biological properties of virus infection, namely, to overwhelm the cell over a time frame within which the cell cannot effectively respond. The observation of concerted expression for the vaccinia proteins (Fig. 2) therefore also serves to internally validate, and serve as a quality control for, the quantitation data set as a whole. While a few vaccinia virus proteins appeared below the median lines in the early/mock distributions (albeit zero expression in the mock sample would be expected to yield an early/mock ratio of no less than 1:1 or no less than the median line), these were all proteins of vanishingly low absolute abundance early in infection, where accuracy in measurement of relative abundance was sensitive to spectral noise. In contrast, those vaccinia virus proteins above the median line were of adequate abundance for accurate quantitation. In Fig. 2, the monopeptide distributions mirrored the multipeptide ones, indicating that, despite the lower confidence that might be expected for the monopeptide data, credible information was present. Since proteins that are identified on the basis of just one peptide species tend to be of lower abundance in the cell (see discussion of exponentially modified protein abundance index [emPAI], below),

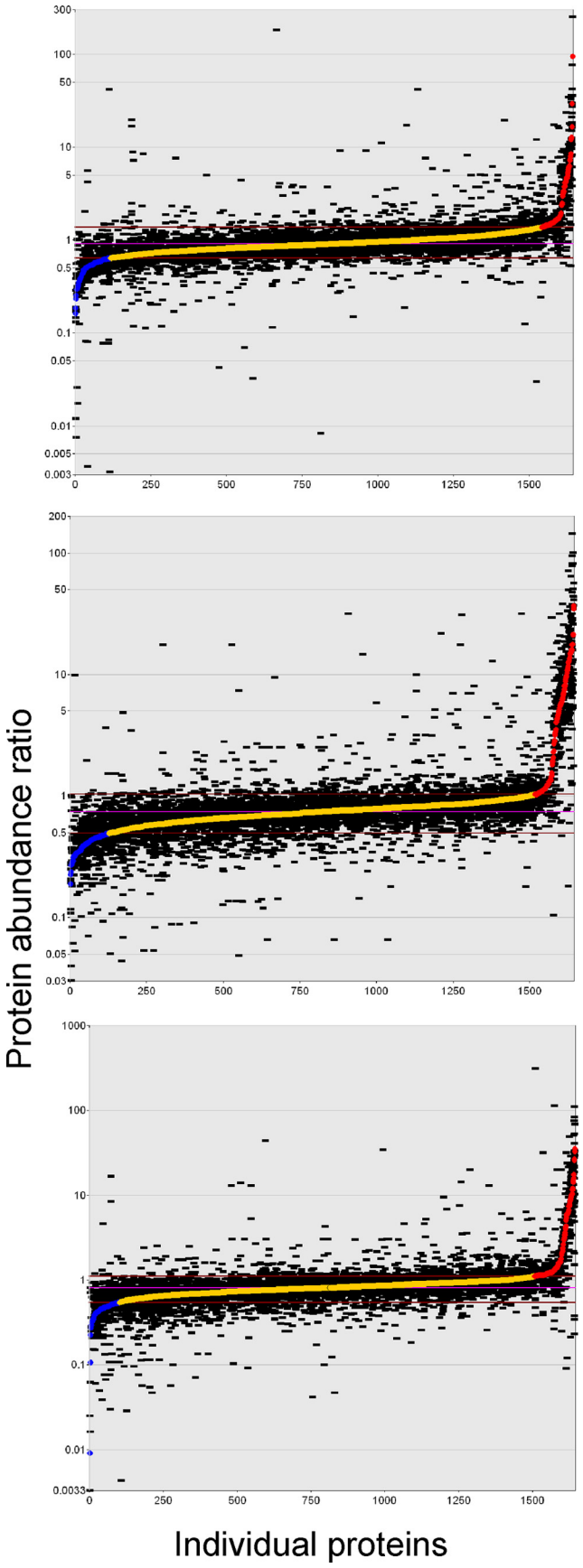

perhaps serving some of the more interesting (e.g., regulatory) roles, the monopeptide data were considered worthy of inclusion.

To address protein absolute abundance within the infected cell, all quantitated accessions in this study (human and vaccinia virus) were sorted in order of decreasing emPAI score (an approximation of protein absolute abundance on the basis of protein coverage (26) (Fig. 3). Vaccinia virus accessions were found throughout the range of emPAI scores (Fig. 3), consistent with vaccinia virus proteins occupying a wide range of absolute abundances in the infected cell up to and including the most abundant. Assuming the cellular proteins detected here represent, very approximately, the top ~30% most abundant proteins in the cell (see above), then the expressed vaccinia virus proteins appear to occupy at least this range of abundances. Many of the vaccinia virus gene products not detected might be present but at lower abundance.

As a result of various studies over the past 30 or more years, vaccinia virus genes have been classified as either early, intermediate, or late (or various combinations thereof, such as early/late or early/intermediate). These studies are based on either predicted time of mRNA synthesis (e.g., promoter prediction [14, 15]), mRNA steady-state levels (nuclease S1, primer-extension analysis, or deep sequencing) (see the introduction), time of protein synthesis (^{35}S metabolic labeling), or steady-state protein level (immunoblotting). Complicating factors in extrapolating some of the prior studies to steady-state protein levels in the cell include the following: unknown mRNA and protein turnover rates (half-lives), polycistronic late mRNAs covering neighboring early genes (due to the absence of late gene termination signals), the detection of protein from input virus early during infection despite an absence of early synthesis, and the interpretation of a drop in mRNA levels as either gene shutoff or a switch to a weaker promoter of a different class. In this regard, a mixture of criteria appears to have been used to define the "known" expression class by the Poxvirus Bioinformatics Resource Center (http://www.poxvirus.org/vaccinia_orthologs.asp).

Despite the limited time course information available in the current study, i.e., just two time points, these data provided an opportunity to examine the expression kinetics of 104 vaccinia virus gene products during infection independently yet in an in-

FIG 1 Global quant ratio distributions after filtering for multipeptide-only. Early/mock (top), late/mock (middle), and late/early (bottom). The *y* axis (log scale) shows protein abundance ratio. On the *x* axis, each overlapping colored spot represents an individual protein. Faint magenta line (close to $y = 1.0$) represents the median ratio for the whole distribution; faint brown lines indicate 10th and 90th percentiles (10% of the total *x* count combined from multi- and monopeptide distributions exceeded these *y* values). Blue/red spots indicate *y* values below 10th/above 90th percentile, respectively. Remaining spots are shown in yellow. Median and percentiles were used as opposed to absolute ratio values in order to normalize potential effects of compositional differences between the original protein samples. Black bars represent individual peptide species. The figure tends to overstate the influence of outlying peptide species because (i) very abundant peptides clustering around the mean are piled up in the figure and hard to distinguish and (ii) peptide species clustering close to the mean were frequently represented by multiple acquisitions (typically from various chromatographic fractions), with outliers often represented by just one acquisition. The few outlying peptide species remaining after filtering, particularly those arising from multiple acquisitions whose individual quantitation values clustered (even when from distinct chromatographic fractions), are considered likely to represent distinct, as yet uncharacterized, protein isoforms of outlying abundance.

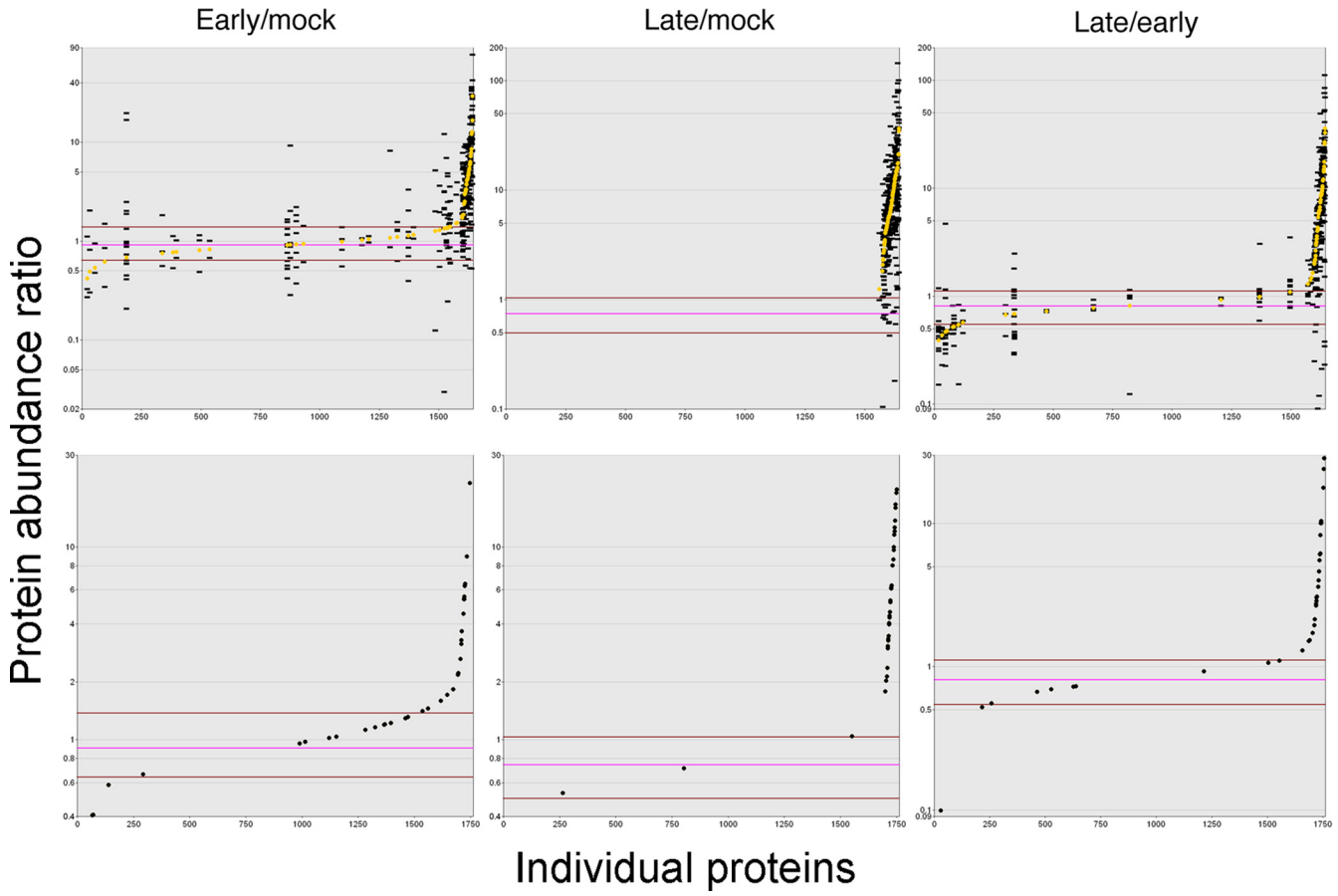

FIG 2 Quant ratio distributions as described for Fig. 1 but with host cell accessions stripped away and showing the vaccinia virus-encoded proteins only. Upper panels shows multipeptide quant ratio distributions; lower panels show monopeptide quant ratio distributions. Other details are as described for Fig. 1, except that all individual accession means are shown in yellow.

ternally consistent manner. The 104 quantitated vaccinia virus proteins could be quite clearly assigned to four kinetic classes (schematized in Fig. 4A; see also Fig. S2 in the supplemental material for raw data on all 104 proteins), as follows: class 1, present early, less abundant late; class 2, present early, equivalent abundance late; class 3, present early, more abundant late; class 4, no apparent expression early, expressed late. Of the 104 vaccinia virus proteins, 22 were found in kinetic class 1, 7 were in kinetic class 2, 41 were in class 3, and 31 were in class 4. Three could not be conclusively assigned (see Fig. S2).

The expression kinetics data were interpreted in the context of predicted and experimental expression data as listed by the Poxvirus Bioinformatics Resource Center (http://www.poxvirus.org/vaccinia_orthologs.asp and references therein) and also in the context of the recently reported vaccinia virus transcriptome map (63). In terms of predicted expression class (i.e., apparent promoter type listed at the above website), there was a noticeable correlation with our protein kinetic class data (Fig. 4B), namely, of class 1 with early (68%) and early/late (32%) promoters, class 2 with (almost entirely) early/late promoters, class 3 with early/late promoters (61%) and true late promoters (32%), and class 4 almost entirely with true late promoters. In terms of the recently reported experimental vaccinia virus transcriptome map, there was an even tighter correlation of our protein expression classes with transcript class (albeit the transcriptome map indicated only earliest detected mRNA expression), namely, of classes 1 and 2 both with vaccinia virus early transcripts (100%) of class 3 with, predominantly, early (51%) and intermediate (34%) transcripts (only the remaining 15% were true late transcripts), and class 4 predominantly with intermediate (45%) and late (48%) transcripts, with just 6% of class 4 transcripts being considered early. This remarkable correlation of *de facto* protein steady-state levels with the transcriptome map indicated that the transcript is the main driver of steady-state protein levels and reaffirmed the accurate assignment of transcripts broadly.

In terms of known expression data (via mixed criteria and based on older studies, as listed at http://www.poxvirus.org/vaccinia_orthologs.asp), a relationship was still apparent, with early and early/late genes well represented in classes 1 to 3 and true late proteins appearing in classes 3 and 4, as might be expected (Fig. 4D). Nonetheless, the correlation was weaker than for transcript and promoter class, with a number of unknowns. The small number of genes/proteins classified as intermediate were represented largely in kinetic class 3 (until very recently, the number of genes known to be expressed at the intermediate stage was very small [63]). The block of nominally early-only genes found in our protein kinetic class 3 (Fig. 4D) indicates the possibility of their misassignment in older studies due to an inability to detect a con-

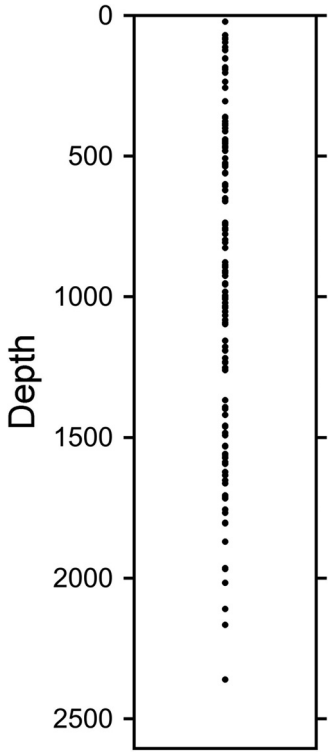

FIG 3 Abundance dynamic range of vaccinia virus proteins extends at least through the detected portion of the infected cell proteome. All quantitated accessions in this study (human and vaccinia virus) were sorted in order of decreasing emPAI score (26). The *y* axis represents the position in the sorted list in which 0 indicates the protein with highest emPAI score and increasing *y* values represent increasing depth (decreasing abundance, or emPAI). Each position in the descending sort occupied by a vaccinia virus accession is indicated by a solid black sphere. emPAI scores are a function of numbers of peptides detected for a protein. Since the likelihood of a precursor being targeted for MS/MS relates to the intensity of the most abundant member of its isotopic labeling triplet, emPAI relates to the protein sample in which it is most abundant.

tinued protein accumulation late in infection and/or the possible presence of secondary, intermediate, or late promoter elements that remain undetected (63).

Figure 4E correlates our four protein kinetic classes with packaging data compiled from published virion proteome studies (9, 46, 64) along with our own virion proteome experiments (unpublished). In terms of virion packaging, our protein kinetics were, again, close to those expected: proteins known to be packaged on the basis of virion proteome analysis (9, 46, 64; also our unpublished virion proteome) were represented largely in classes 3 and 4, while proteins never detected in the virion were found largely in class 1. Thus, proteins whose abundance decreases late during infection are rarely packaged, as might be expected.

Host cell gene products at ends of quant ratio distributions. Our initial analysis of host cell (human) proteins focused on the ends of the quant ratio distributions. As mentioned above, for each quant ratio (early/mock, late/mock, and late/early), the 3,403 proteins that could be quantitated were split into multipeptide and monopeptide distributions. As indicated in Table S2 in the supplemental material, between 103 and 127 of the 340 accessions falling outside the 10th and 90th percentiles, respectively, were multipeptide. The resulting list of 474 multipeptide accessions from the early/mock and late/mock distributions were culled to remove vaccinia virus proteins along with host cell accessions whose visually confirmed peptide species spanned a range of quant ratios with no consensus. Finally, for any isoform families clearly identifiable from protein descriptors, redundant accessions and those with unknown function were culled. The remaining 190 host proteins or protein isoform families could be manually annotated into 39 broad functional categories (see Fig. S3 in the supplemental material). Summation of numbers of proteins from the distribution ends falling in each functional category (Fig. 5) shows great unevenness from category to category. Taking five as a mean count per category if the distribution were even, the following 10 classes contained more than the mean number of members: cytoskeletal (18 total, up or down, early or late), defense (8 total, up or down, early or late), energy (24 total, almost entirely down, early and late), mRNA binding/RNA unwinding (12 total, 60% up and 40% down, early or late), mRNA splicing (7 total, all up, early and late), protein folding (15 total, nearly all down, early or late), protein trafficking (12 total, mostly down, early), protein turnover (18 total, mostly down, early and late), ribosomal (15 total, all down, early and late), and signal transduction (18 total, 75% of them down, early or late). These 10 classes dominated the overall count, sharing 144 accessions, or 69% of the total accession count. Coadding the groups mRNA splicing, mRNA processing/maturation, and mRNA translatability/exon junction complex ([EJC] all three were predominantly splicing related) gives a combined count of 13, almost exclusively up in abundance as a result of infection. Including the category mRNA binding/RNA unwinding would bring the count to 26 (approximately half up and half down). In this manner, 18% of all proteins in Fig. 5 seem to be involved in mRNA processing of some sort, including splicing.

All host cell gene products. In order to cover not only the ends of distributions in the host cell proteome but, instead, the complete host protein data set, the latter was analyzed in the context of the Gene Ontology (GO) tree (www.geneontology.org). After a batch search at that website in which each host accession in our experimental data set was annotated with all applicable GO terms, PDMQ software (Materials and Methods) was used to decorate all 31,968 nonobsolete nodes of the entire GO tree with the six quant ratio values attributable to each relevant accession from the GO batch search, providing, for each populated node, six GO term-specific quant ratio distributions. If any of the three multipeptide distributions for a GO term was skewed such that there was a >2.5-fold greater number of accessions on one side than the other of the median quant ratio for the global distribution of all accessions for the experiment and if the GO term was associated with more than nine accessions in total, then the GO term was bookmarked.

At the end of this analysis, 5,981 of the 31,968 GO terms had host cell accessions assigned to them, of which 497 were biased (skewed) according to the above criteria. Of these, 376 were visually selected as being notable, eliminating any containing, for example, strings of identically valued isoforms and/or GO terms that were too abstract to be interpretable. The 376 GO terms were sorted manually into broad functional categories (see Fig. S4 in the supplemental material), among which there were clear indications of functional category-specific biases in host protein abundance during infection. Most notably, for example, the block of red covering the energy class (Fig. S4, rows 71 to 107) indicates that infection is suppressing levels of

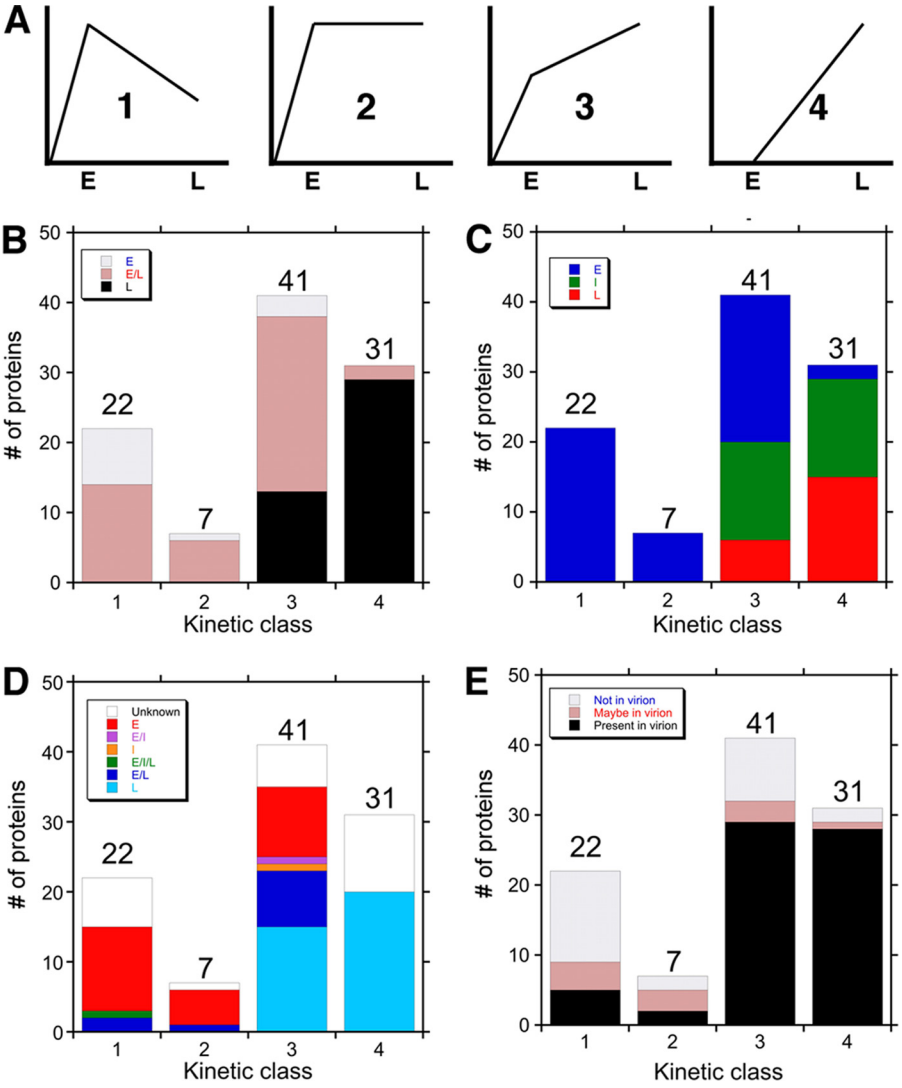

FIG 4 Vaccinia virus proteins. Correlation of the four kinetic classes with predicted and actual expression and packaging data. (A) Depiction of the four kinetic classes: E, early; L, late. (B to E) Breakout of confidently quantitated vaccinia virus proteins in each of the four kinetic classes genes on the basis of: predicted promoter type for the protein's genes in the vaccinia virus genome (B), the vaccinia virus transcriptome map (63) (C), experimental expression data of various types as discussed in the text (D), and presence within the virion (E). Protein classes are identified according to the legends on the panels: E, early; I, intermediate; L, late.

a broad variety of proteins involved in energy metabolism early in infection and that these remain suppressed. In Fig. S4, the signal transduction, Neuronal, and Protein degradation categories also showed large blocks of red both early and late in infection. Protein quant ratios associated with defense-related GO terms were also skewed toward underabundance at some point during infection. Protein quant ratios associated with nucleotide metabolism and ion-related GO terms seemed to be largely skewed toward underabundance early in infection, with many of these returning closer to uninfected cellular levels late.

In contrast, other groups of proteins were increased in abundance as a result of infection. Proteins assignable to GO terms in the developmental/differentiation category were mainly increased in abundance late in infection with respect to early in infection, and proteins assignable to GO terms in the DNA/chromatin class were largely overabundant late in infection with respect to either early or mock. Proteins assignable to vesicular transport GO terms were also generally overabundant during infection. Proteins assignable to GO terms in the cytoskeleton category, including actin-related GO terms, seemed to be overabundant (especially late during infection), with the exception of microtubular GO terms whose distributions were largely skewed toward underabundance. Within each of the above broad functional categories, some protein accessions were shared between individual GO terms, with redundancy varying from ~1.4-fold to ~4-fold, depending on the group (data not shown).

DISCUSSION

Here, we have addressed the steady-state homeostasis of intracellular proteins (nuclear and cytoplasmic, host cell, and viral) during vaccinia virus infection via mass spectrometry, using dimethyl

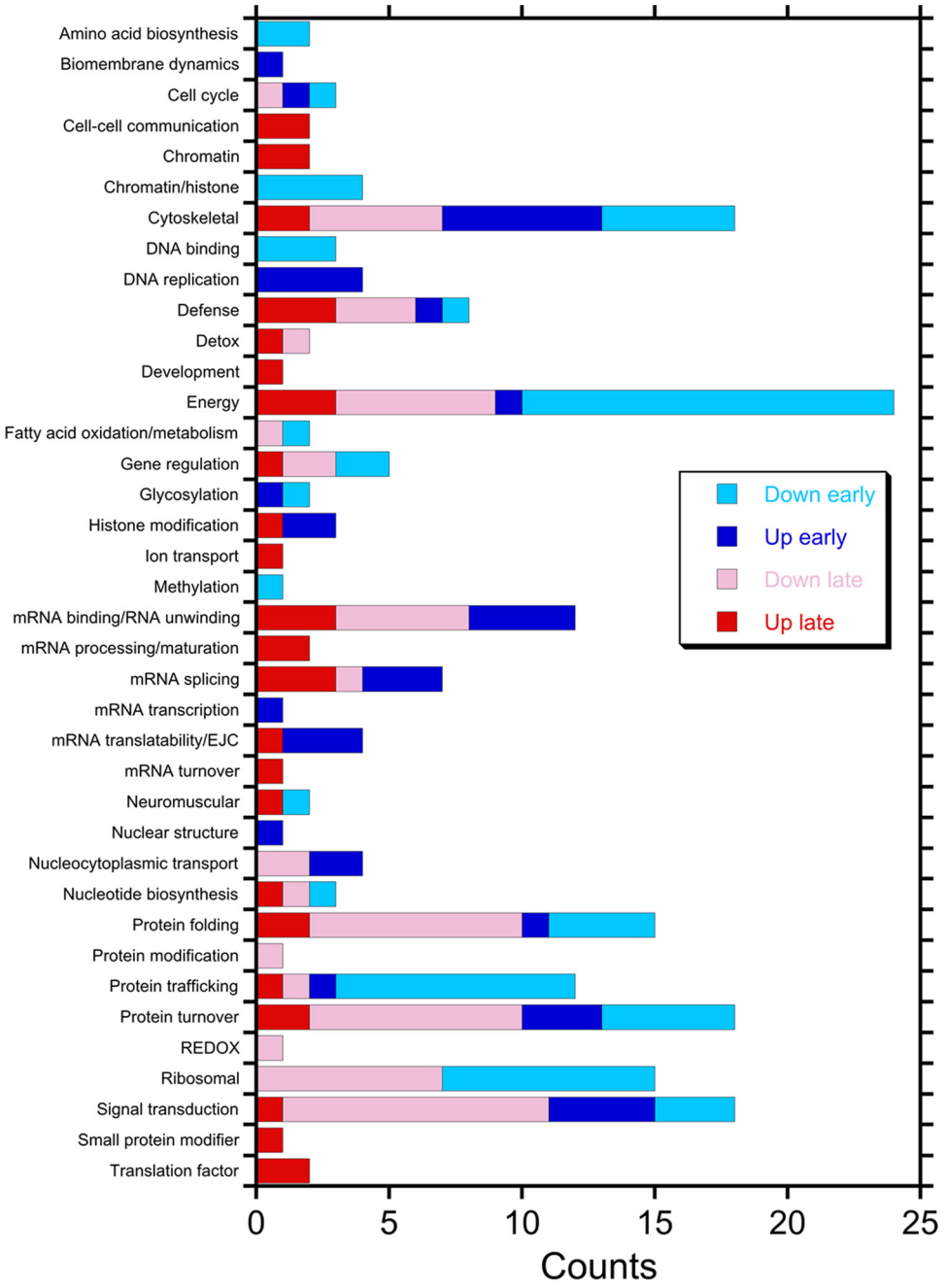

FIG 5 Analysis of host (human) infected-cell gene products at the ends of the early/mock and late/mock distributions (below 10th/above 90th percentile by relative quantitation ratio), according to protein functional category (*y*). The *x* axis shows number of gene products assignable to the function, as indicated on the figure. Down, underabundant; up, overabundant.

isotopic tagging and precursor-level quantitation. A total of 136 virus-encoded proteins present in the infected cell (~64% of the vaccinia virus genome) were addressable, alongside the products of 3,798 host cell genes (~16.5 to 18% of the human genome) (10, 42). These totaled approximately 4,326 IPI-human/vaccinia virus protein accessions or, very approximately, 30% of the infected cell proteome. Given that our approach availed just three quantitation channels, only two time points were employed here. This necessitated the use of a DNA replication inhibitor in the early culture in order to provide a clear distinction of early from late time points, which may have been avoidable in the context of a multi-time point study. The inhibitor used was AraC, following its widespread use in vaccinia virus molecular biology. AraC and its metabolites have been documented to inhibit DNA and RNA polymerases, ribonucleotide reductase, and DNA damage repair mechanisms (6) and to damage RNA and DNA into which it or its metabolites are incorporated (33). It may also influence some signal transduction pathways (53). With insufficient quantitation channels for inclusion of a control of uninfected cells incubated with AraC, we could not entirely discount cellular responses to

AraC. Such responses, however, would be detected as a change in the quant ratio in the early (AraC-treated) sample but not in the late (untreated) sample. Such kinetics were noted for only a few proteins (some of which have known roles in cellular DNA replication [data not shown]) and not in the broad mass of proteins quantitated herein. Importantly, given the good correspondence between the deduced kinetics of vaccinia virus proteins here and the known kinetics of a large number of these proteins (Fig. 4B to D) (discussed further below), the results of the study provided excellent internal validation for our quantitation data. It is also notable that the protein dynamics occurring upon vaccinia virus infection that were observed in multipeptide distributions were reflected also in the monopeptide distributions (Fig. 2), indicating that even the latter contained useful quantitative information.

In this study, we performed relative (as opposed to absolute) quantitation, starting with equivalent total protein amounts from each of the three samples to compensate for potential cell loss. Under these conditions, progression from cellular to viral programming, accompanied by a global and proportionate downregulation of all cellular proteins, could potentially have been compensated for by the methodology and therefore be undetectable. Such a mechanism seems very unlikely, however, given the wide diversity of protein half-lives documented in the mammalian cell (51) (see below).

With regard to the vaccinia virus gene products, four kinetic classes were discerned (see Results). In the context of just two infected cell samples, the observation of four kinetic classes should not be interpreted as indicating that four distinct temporal phases of protein expression are present during infection but, instead, that four combinations of the known pre- and postreplicative phases were apparent. Kinetic classes 1 and 2 were candidates for the products of vaccinia virus early genes, in which class 2 represented highly stable (long-lived) vaccinia virus early proteins and/or the products of early/intermediate and/or early/late mRNA expression (this point could be clarified by either metabolic protein labeling or transcriptional studies or in the context of deep-sequencing studies [61, 63]). Due to the use of 20-h expression in the presence of AraC, with prolongation of the vaccinia virus early phase, the possibility cannot be entirely discounted that early proteins overaccumulate, such that true class 3 proteins take on class 2 character, and true class 2 proteins take on class 1 character. Nonetheless, the kinetic classes observed were strikingly consistent with the recently published vaccinia virus transcriptome map. The relatively small number of class 2 products indicates that there may not be a major role for long-lived, early-only expressed proteins in the vaccinia virus life cycle. Moreover, all of the early proteins showed some presence late: no kinetic class was detected of vaccinia virus proteins showing a burst of early protein expression and then returning to mock levels late in infection. Therefore, no evidence was found here for a mechanism, or role, for the complete elimination of early vaccinia virus gene products late during infection. Although the high multiplicity used in this study raised the possibility that some exclusively late genes may have been present among classes 1 to 3, with the early detection of these proteins arising solely from input virion, there was, nonetheless, a good correlation between kinetic class and promoter type and a dramatic correlation with the transcriptome map (see Results).

With regard to host cell proteins, it was initially hypothesized that vaccinia virus may downregulate the levels/activities of specific host proteins that could hinder virus replication and/or, in response to infection, that the host cell may upregulate levels/activities of its own proteins in order to hinder virus replication. Host steady-state protein levels could potentially be modulated via mRNA synthesis, mRNA stability, protein synthesis, or protein stability. In fact, vaccinia virus is known to effect a rapid and profound decrease in rates of host cell protein synthesis (19, 39), with a switch to virus protein synthesis via two of these four effects, namely, a shutdown of host mRNA synthesis (see reference 38 and references therein), coupled with the accelerated degradation of host cell mRNA (5, 11). While these two effects are doubtless key to the rapid dominance of virus protein synthesis, it is hard to envisage them being able to elicit profound changes in the infected cell steady-state proteome, given that infectious virus starts to appear 6 to 8 h after infection in one-step growth curve experiments in cell culture, with no new virus being produced after 20 h (20); moreover, profound cellular morphological changes are visible after just 1 to 1.5 h (see below), whereas the median half-life of mammalian fibroblast proteins mostly covers much longer timescales, in the range 10 to 300 h, with a median of half-life 46 h (51). Consistent with this, the decisive changes in vaccinia virus protein dynamics (Fig. 2) were set against the backdrop of a broadly stable host cell proteome. A minor fraction of the host cell proteins, however (~369, or ~8.7% of the characterized proteome), fell outside the 10th/90th percentiles of the global quant ratio distributions after exhaustive quality filtering and inspection. GO term-specific trends were also noticeable. Specific proteins, therefore, may undergo more sudden or profound changes in abundance during infection. Given the relatively long half-lives of cellular proteins (see above), this group could represent a subset of host cell proteins possessing unusually short natural half-lives, coupled with global cellular mRNA loss. Nonetheless, it would seem to be in the virus's interest to possess a mechanism for the destabilization of targeted proteins, especially given the opportunities for this afforded by a relatively large virus genome. In this regard, it has been reported that poxvirus ankyrin repeat proteins associate with cellular SCF1 ubiquitin ligase complexes, forming a unique class of F-box proteins (52).

A basis can be argued for many of the functional category-specific changes in host cell steady-state protein levels detected here upon infection. For example, with regard to the cytoskeletal proteins, the constitutive cytopathic effect (CPE) of poxvirus infection is associated with radical morphological changes, including cell rounding, which occur within just 1 to 1.5 h of infection (28), not to mention cell-cell dissociation and migration (3). Cell rounding, which is independent of the replication status of the infecting virus (3, 22) is associated with alterations in actin and intermediate filaments and microtubules (see reference 38 and references therein). Macropinocytotic virus entry is also associated with changes in cytoskeletal actin (37). Moreover, vaccinia virus actively polymerizes actin tails late during infection (13) and employs microtubules for virion exit (56). While cytoskeletal effects could be accounted for on the basis of cytoskeletal depolymerization/rearrangements without necessarily requiring changes in cytoskeletal protein levels, nonetheless, cytoskeletal proteins were highly represented at the ends of quant ratio distributions both early and late during infection (Fig. 5). Moreover, with the exception of microtubule-related GO terms whose members' quant ratios were skewed toward underabundance upon infection, quant ratios for the other cytoskeletal (notably actin)-related

GO terms tended to be skewed toward overabundance (see Fig. S3 in the supplemental material). Therefore, rational proteomic correlates have been detected for the rapid and dramatic changes in cell morphology early and late during infection.

mRNA binding/RNA unwinding proteins were highly represented here at distribution ends, as were proteins involved in mRNA splicing and in mRNA maturation and translatability in general. Perhaps consistent with this, there is a recurrent theme of ribonucleoprotein involvement in vaccinia virus intermediate and late transcription, with reports of hnRNP A2/B1 and RBM3 activation of a late promoter *in vitro* (16, 60), and the demonstration of G3BP and CAPRIN-1 involvement in intermediate transcription (31, 48, 49) (G3BP has endoribonuclease/unwinding activity; CAPRIN-1 has a role in the transport and translation of mRNAs.) With regard to defense-related proteins, distribution ends featured these, and defense-related GO terms were also mainly underabundant at some point during infection. It would be no surprise that vaccinia virus infection is associated with changes in defense-related protein homeostasis. With regard to signal transduction, signal transduction-related proteins were well-represented at the distribution ends, and signal transduction-related GO terms showed large blocks of red both early and late in infection in Fig. S3 in the supplemental material. It is not unexpected that the virus would interact with signal transduction pathways, and such interactions have been well documented (2, 7, 12, 17, 40, 44, 45, 57). Moreover, changes in the mRNAs of cellular signal transduction proteins upon vaccinia virus infection have also been reported (21, 34; see also the introduction). With regard to protein trafficking, protein trafficking-related proteins were well represented at the distribution ends, and proteins belonging to vesicular transport-related GO categories were generally overabundant during infection. This is not inconsistent with the site of poxvirus replication in cytoplasmic factories at the nuclear membrane/ER nexus, and the roles played by the trans-Golgi or endosomal cisternae in providing membranes for the wrapping of nascent virus during transport to the cell surface (23, 25, 47, 50, 54) as well as interaction of vaccinia virus with the macropinocytotic pathway during entry (24, 36, 55). The downregulation of general protein turnover mechanisms (mainly proteasome and ubiquitin pathway-related proteins) was prevalent at distribution ends, along with GO term skews, showing large blocks of red both early and late in infection in Fig. S3. This would be consistent with the rapid accumulation of virus proteins during infection, coupled with a possible switch to a more targeted approach to the degradation of specific proteins (see above). With regard to the GO term category DNA/chromatin, skews were largely toward overabundance later in infection with respect to either the early or mock infection. This is consistent with the increased mRNA levels for core histone genes found in microarray studies of rabbitpox-infected cells and the finding of chromatin packaging and remodeling as an overrepresented category by deep-sequencing of the poly(A)$^+$ transcriptome of vaccinia virus-infected HeLa cells (8, 62; see also the introduction). Of the 58 cellular transcripts specifically identified in the infected-cell deep-sequencing study (62), the product of only one, SLC1A5, was present in our data set (registering a mild overabundance late with respect to early).

Perhaps more of a surprise than the above was the prevalence of energy-related proteins at distribution ends (almost entirely down in abundance, both early and late) (Fig. 5), along with the consistent downward skewing of energy-related GO terms (see Fig. S3 in the supplemental material). Also somewhat counterintuitive was the apparent decrease in abundance of ribosomal proteins and proteins involved in protein folding (distribution ends analysis). Since rapid virus production might be expected to favor energy production, protein folding, and abundant ribosomes, perhaps these more unexpected changes arise as secondary effects or host cell responses that may be multiplexed or overlaid with infection, such as necrosis (and the associated breakdown of membrane integrity and small molecule feedback and collapse of ion gradients, etc.) or the mitochondrion-centered processes of apoptosis. Intercellular signaling effects might also be at play. Changes related to protein folding and translation could, perhaps, be related to the concentration of some translation initiation factors and ribosomal proteins within cytoplasmic virus factories (30). Moreover, it is notable that at least one ribosomal protein, namely, S30, whose change in abundance (down) was the most marked of any host cell protein in the early/mock distribution, and which was the most markedly changed in abundance of any of the ribosomal proteins in any of the distributions (data not shown), has secondary roles as a free protein which are distinct from its role within the ribosome. Specifically, the cellular *FAU* gene, which encodes a ubiquitin-like protein fused to the N terminus of S30, is proapoptotic (29, 43), and a cytoplasmic antimicrobial peptide termed ubiquicidin is identical to ribosomal protein S30 (29, 58), consistent with a role of S30 in cellular defense. Other ubiquitin-ribosomal protein fusions in the current proteome were not so markedly changed in abundance due to infection (data not shown).

In summary, the current study has examined changes in vaccinia virus and cellular protein levels early and late during infection and provides a point of reference for the further study of intracellular protein homeostasis in the poxvirus-infected cell.

ACKNOWLEDGMENTS

We thank M. Buchmeier for permission to use his lab for cell culture, Kristeene Knopp for seeding cells, and Andrew Mercer for bringing our attention to his work on ankyrin repeat proteins. We thank the UCI Center for Virus Research for encouragement.

This work was unsupported.

REFERENCES

1. **Almen MS, Nordstrom KJ, Fredriksson R, Schioth HB.** 2009. Mapping the human membrane proteome: a majority of the human membrane proteins can be classified according to function and evolutionary origin. BMC Biol. **7**:50.
2. **Arakawa Y, Cordeiro JV, Schleich S, Newsome TP, Way M.** 2007. The release of vaccinia virus from infected cells requires RhoA-mDia modulation of cortical actin. Cell Host Microbe **1**:227–240.
3. **Bablanian R, Baxt B, Sonnabend JA, Esteban M.** 1978. Studies on the mechanisms of vaccinia virus cytopathic effects. II. Early cell rounding is associated with virus polypeptide synthesis. J. Gen. Virol. **39**:403–413.
4. **Boersema PJ, Raijmakers R, Lemeer S, Mohammed S, Heck AJ.** 2009. Multiplex peptide stable isotope dimethyl labeling for quantitative proteomics. Nat. Protoc. **4**:484–494.
5. **Boone RF, Moss B.** 1978. Sequence complexity and relative abundance of vaccinia virus mRNA's synthesized in vivo and in vitro. J. Virol. **26**: 554–569.
6. **Braess J, et al.** 1999. Leukaemic blasts differ from normal bone marrow mononuclear cells and CD34$^+$ haemopoietic stem cells in their metabolism of cytosine arabinoside. Br. J. Haematol. **105**:388–393.
7. **Brown JP, Twardzik DR, Marquardt H, Todaro GJ.** 1985. Vaccinia virus encodes a polypeptide homologous to epidermal growth factor and transforming growth factor. Nature **313**:491–492.
8. **Brum LM, Lopez MC, Varela JC, Baker HV, Moyer RW.** 2003. Microar-

ray analysis of A549 cells infected with rabbitpox virus (RPV): a comparison of wild-type RPV and RPV deleted for the host range gene, SPI-1. Virology **315**:322–334.
9. **Chung CS, et al.** 2006. Vaccinia virus proteome: identification of proteins in vaccinia virus intracellular mature virion particles. J. Virol. **80**: 2127–2140.
10. **Clamp M, et al.** 2007. Distinguishing protein-coding and noncoding genes in the human genome. Proc. Natl. Acad. Sci. U. S. A. **104**: 19428–19433.
11. **Cooper JA, Moss B.** 1979. In vitro translation of immediate early, early, and late classes of RNA from vaccinia virus-infected cells. Virology **96**: 368–380.
12. **Cordeiro JV, et al.** 2009. F11-mediated inhibition of RhoA signalling enhances the spread of vaccinia virus in vitro and in vivo in an intranasal mouse model of infection. PLoS One **4**:e8506.
13. **Cudmore S, Cossart P, Griffiths G, Way M.** 1995. Actin-based motility of vaccinia virus. Nature **378**:636–638.
14. **Davison AJ, Moss B.** 1989. Structure of vaccinia virus early promoters. J. Mol. Biol. **210**:749–769.
15. **Davison AJ, Moss B.** 1989. Structure of vaccinia virus late promoters. J. Mol. Biol. **210**:771–784.
16. **Dellis S, et al.** 2004. Protein interactions among the vaccinia virus late transcription factors. Virology **329**:328–336.
17. **Dodding MP, Way M.** 2009. Nck- and N-WASP-dependent actin-based motility is conserved in divergent vertebrate poxviruses. Cell Host Microbe **6**:536–550.
18. **Earl PL, Cooper N, Wyatt LS, Moss B, Carroll MW.** 2001. Preparation of cell cultures and vaccinia virus stocks, p 16.16.1–16.16.3. *In* Ausubel FM (ed), Current protocols in molecular biology. Wiley Interscience, New York, NY.
19. **Esteban M, Metz DH.** 1973. Early virus protein synthesis in vaccinia virus-infected cells. J. Gen. Virol. **19**:201–206.
20. **Furness G, Youngner JS.** 1959. One-step growth curves for vaccinia virus in cultures of monkey kidney cells. Virology **9**:386–395.
21. **Guerra S, et al.** 2003. Cellular gene expression survey of vaccinia virus infection of human HeLa cells. J. Virol. **77**:6493–6506.
22. **Hanson CV.** 1992. Photochemical inactivation of viruses with psoralens: an overview. Blood Cells **18**:7–25.
23. **Hiller G, Weber K.** 1985. Golgi-derived membranes that contain an acylated viral polypeptide are used for vaccinia virus envelopment. J. Virol. **55**:651–659.
24. **Huang CY, et al.** 2008. A novel cellular protein, VPEF, facilitates vaccinia virus penetration into HeLa cells through fluid phase endocytosis. J. Virol. **82**:7988–7999.
25. **Husain M, Moss B.** 2003. Evidence against an essential role of COPII-mediated cargo transport to the endoplasmic reticulum-Golgi intermediate compartment in the formation of the primary membrane of vaccinia virus. J. Virol. **77**:11754–11766.
26. **Ishihama Y, et al.** 2005. Exponentially modified protein abundance index (emPAI) for estimation of absolute protein amount in proteomics by the number of sequenced peptides per protein. Mol. Cell Proteomics **4**:1265–1272.
27. **Ishihama Y, Rappsilber J, Mann M.** 2006. Modular stop and go extraction tips with stacked disks for parallel and multidimensional Peptide fractionation in proteomics. J. Proteome Res. **5**:988–994.
28. **Joklik WK.** 1966. The poxviruses. Bacteriol. Rev. **30**:33–66.
29. **Kas K, Michiels L, Merregaert J.** 1992. Genomic structure and expression of the human fau gene: encoding the ribosomal protein S30 fused to a ubiquitin-like protein. Biochem. Biophys. Res. Commun. **187**:927–933.
30. **Katsafanas GC, Moss B.** 2007. Colocalization of transcription and translation within cytoplasmic poxvirus factories coordinates viral expression and subjugates host functions. Cell Host Microbe **2**:221–228.
31. **Katsafanas GC, Moss B.** 2004. Vaccinia virus intermediate stage transcription is complemented by Ras-GTPase-activating protein SH3 domain-binding protein (G3BP) and cytoplasmic activation/proliferation-associated protein (p137) individually or as a heterodimer. J. Biol. Chem. **279**:52210–52217.
32. **Kotwal GJ, Moss B.** 1988. Analysis of a large cluster of nonessential genes deleted from a vaccinia virus terminal transposition mutant. Virology **167**:524–537.
33. **Kufe DW, Major PP.** 1982. Studies on the mechanism of action of cytosine arabinoside. Med. Pediatr. Oncol. **10**(Suppl 1):49–67.
34. **Ludwig H, et al.** 2005. Role of viral factor E3L in modified vaccinia virus Ankara infection of human HeLa Cells: regulation of the virus life cycle and identification of differentially expressed host genes. J. Virol. **79**: 2584–2596.
35. **Mense SM, et al.** 2006. Gene expression profiling reveals the profound upregulation of hypoxia-responsive genes in primary human astrocytes. Physiol. Genomics **25**:435–449.
36. **Mercer J, Helenius A.** 2008. Vaccinia virus uses macropinocytosis and apoptotic mimicry to enter host cells. Science **320**:531–535.
37. **Mercer J, Helenius A.** 2009. Virus entry by macropinocytosis. Nat. Cell Biol. **11**:510–520.
38. **Moss B.** 2007. Poxviridae: the viruses and their replication, p 2905–2946. *In* Knipe DM, et al. (ed), Fields virology, 5th ed. Lippincott Williams & Wilkins, Philadelphia, PA.
39. **Moss B, Salzman NP.** 1968. Sequential protein synthesis following vaccinia virus infection. J. Virol. **2**:1016–1027.
40. **Newsome TP, Scaplehorn N, Way M.** 2004. SRC mediates a switch from microtubule- to actin-based motility of vaccinia virus. Science **306**: 124–129.
41. **Niles EG, et al.** 1986. Nucleotide sequence and genetic map of the 16-kb vaccinia virus HindIII D fragment. Virology **153**:96–112.
42. **Pertea M, Salzberg SL.** 2010. Between a chicken and a grape: estimating the number of human genes. Genome Biol. **11**:206.
43. **Pickard MR, Mourtada-Maarabouni M, Williams GT.** 2011. Candidate tumour suppressor Fau regulates apoptosis in human cells: An essential role for Bcl-G. Biochim. Biophys. Acta **1812**:1146–1153.
44. **Postigo A, Cross JR, Downward J, Way M.** 2006. Interaction of F1L with the BH3 domain of Bak is responsible for inhibiting vaccinia-induced apoptosis. Cell Death Differ. **13**:1651–1662.
45. **Postigo A, Martin MC, Dodding MP, Way M.** 2009. Vaccinia-induced epidermal growth factor receptor-MEK signalling and the anti-apoptotic protein F1L synergize to suppress cell death during infection. Cell Microbiol. **11**:1208–1218.
46. **Resch W, Hixson KK, Moore RJ, Lipton MS, Moss B.** 2007. Protein composition of the vaccinia virus mature virion. Virology **358**:233–247.
47. **Risco C, et al.** 2002. Endoplasmic reticulum-Golgi intermediate compartment membranes and vimentin filaments participate in vaccinia virus assembly. J. Virol. **76**:1839–1855.
48. **Rosales R, Sutter G, Moss B.** 1994. A cellular factor is required for transcription of vaccinia viral intermediate-stage genes. Proc. Natl. Acad. Sci. U. S. A. **91**:3794–3798.
49. **Sanz P, Moss B.** 1998. A new vaccinia virus intermediate transcription factor. J. Virol. **72**:6880–6883.
50. **Schmelz M, et al.** 1994. Assembly of vaccinia virus: the second wrapping cisterna is derived from the trans Golgi network. J. Virol. **68**:130–147.
51. **Schwanhausser B, et al.** 2011. Global quantification of mammalian gene expression control. Nature **473**:337–342.
52. **Sonnberg S, Seet BT, Pawson T, Fleming SB, Mercer AA.** 2008. Poxvirus ankyrin repeat proteins are a unique class of F-box proteins that associate with cellular SCF1 ubiquitin ligase complexes. Proc. Natl. Acad. Sci. U. S. A. **105**:10955–10960.
53. **Sreenivasan Y, Sarkar A, Manna SK.** 2003. Mechanism of cytosine arabinoside-mediated apoptosis: role of Rel A (p65) dephosphorylation. Oncogene **22**:4356–4369.
54. **Tooze J, Hollinshead M, Reis B, Radsak K, Kern H.** 1993. Progeny vaccinia and human cytomegalovirus particles utilize early endosomal cisternae for their envelopes. Eur. J. Cell Biol. **60**:163–178.
55. **Townsley AC, Weisberg AS, Wagenaar TR, Moss B.** 2006. Vaccinia virus entry into cells via a low-pH-dependent endosomal pathway. J. Virol. **80**:8899–8908.
56. **Ward BM, Moss B.** 2001. Vaccinia virus intracellular movement is associated with microtubules and independent of actin tails. J. Virol. **75**: 11651–11663.
57. **Weisswange I, Newsome TP, Schleich S, Way M.** 2009. The rate of N-WASP exchange limits the extent of ARP2/3-complex-dependent actin-based motility. Nature **458**:87–91.
58. **Wiesner J, Vilcinskas A.** 2010. Antimicrobial peptides: the ancient arm of the human immune system. Virulence **1**:440–464.
59. **Wisniewski JR, Zougman A, Nagaraj N, Mann M.** 2009. Universal sample preparation method for proteome analysis. Nat. Methods **6**:359–362.
60. **Wright CF, Oswald BW, Dellis S.** 2001. Vaccinia virus late transcription is activated in vitro by cellular heterogeneous nuclear ribonucleoproteins. J. Biol. Chem. **276**:40680–40686.

61. **Yang Z, Bruno DP, Martens CA, Porcella SF, Moss B.** 2011. Genome-wide analysis of the 5′ and 3′ ends of vaccinia virus early mRNAs delineates regulatory sequences of annotated and anomalous transcripts. J. Virol. **85**:5897–5909.
62. **Yang Z, Bruno DP, Martens CA, Porcella SF, Moss B.** 2010. Simultaneous high-resolution analysis of vaccinia virus and host cell transcriptomes by deep RNA sequencing. Proc. Natl. Acad. Sci. U. S. A. **107**: 11513–11518.
63. **Yang Z, et al.** 2011. Expression profiling of the intermediate and late stages of poxvirus replication. J. Virol. **85**:9899–9908.
64. **Yoder JD, Chen T, Hruby DE.** 2004. Sequence-independent acylation of the vaccinia virus A-type inclusion protein. Biochemistry **43**:8297–8302.